Electronic Supporting Information

A new approach to prepare most active and stable black titania for visible light-assisted hydrogen production

Apurba Sinhamahapatra, Jong-Pil Jeon, and Jong-Sung Yu*

Department of Energy Systems Engineering, DGIST, Daegu, 711-873, Republic of Korea

E-mail: jsyu@dgist.ac.kr

Experimental:

Preparation of reduced black TiO_2

Commercially available nano TiO_2 (CT) was procured from Aldrich and used as it is. Well-mixed sample of TiO_2 and magnesium powder was placed in a tube furnace and then heated at 650 °C for 5 h in the flow of 5% H_2/Ar. After the annealing treatment, the sample was stirred for 24 h in 1.0 M HCl solution. The sample was washed with sufficient amount of water to remove the acid and dried at 80 °C. Different reduced black TiO_2 samples were prepared with varying the molar ratio of TiO_2 and Mg and denoted as BT-X (where X (=0.3, 0.5, 0.6, 0.75 and 1) is the molar ratio of Mg with respect to TiO_2). Different samples are also prepared for comparison study as follows. The CT was annealed under the argon atmosphere at 650°C to study the effect of temperature and Ar atmosphere. The sample is denoted as CT-Ar. The CT was annealed under 5% H_2/Ar atmosphere at 650°C to study the effect of hydrogen. The sample is denoted as CT-H. The CT was annealed in the presence of Mg powder (0.5 mol ratio) under argon atmosphere at 650°C to study the effect of Mg in the absence of H_2. The sample is denoted as BT-0.5-Ar.

Characterizations

Powder X-ray diffraction (XRD) data were recorded using a Rigaku Smartlab diffractometer with Cu-Kα (0.15406 nm) operated at 40 kV and 30 mA at a scan rate of 4° min^{-1}. Raman analysis was carried out using a Raman spectrometer (NICOLET ALMECA XR), manufactured by Thermo Scientific. A 532 nm laser beam was used for excitation. High-Resolution Transmission Electron Microscopy (HR-TEM) images were collected using JEOL FE-2010, operated at 200 kV. The absorption spectra of the samples were recorded by using an Ultraviolet-

Visible-Near Infrared Spectrophotometer (CARY5000) manufactured by Agilent Technology. X-ray photoelectron spectroscopy (XPS) was performed using an ESCALAB 250 XPS System with a monochromated Al Kα (150 W) source. The energy scale is aligned by using the Fermi level of the XPS instrument (4.10 eV versus absolute vacuum value). The magnetic field dependence of magnetization plots of the sample was obtained at room temperature from a magnetic property measurement system (MPMS SQUID VSM) manufactured by Quantum Design. The photoluminescence spectra were obtained from a Cary Eclipse Fluorescence Spectrophotometer (Agilent Technologies). The nitrogen adsorption–desorption isotherms of the samples were measured at -196 °C using a Micromeritics ASAP 2460 accelerated surface area and porosity analyzer after the samples were degassed at 150 °C to 20 mTorr for 12 h. The specific surface area was determined based on Brunauer–Emmett–Teller (BET) method from nitrogen adsorption data in the relative pressure range from 0.05 to 0.2.

Band gap calculation

The band gap of the samples was calculated using Tauc plot of $(\alpha h\nu)^2$ vs $h\nu$, where α is the absorption coefficient, h is Plank constant, ν is the wavenumber. The value of $h\nu$ is obtained by converting the wavelength (λ) value. The energy band gap (Eg) is obtained from the intercept of the extrapolated linear part of the curve with the energy axis. The valence band top position was obtained from the VB XPS plot and conduction band bottom was calculated by subtracting the band gap value. The probable band structure was portrayed in potential vs NHE energy diagram.

Photocatalytic Pt deposition

Desire amount of TiO_2 catalyst was taken in 50 ml 20% methanol-water solution in a closed gas circulation system. An appropriate amount of H_2PtCl_6. $6H_2O$ was added. The UV light irradiation was obtained from a 450 W Xenon lamp and used for the deposition of Pt under Ar atmosphere. The freshly prepared Pt-deposited catalyst was used as it is for further study.

Photocatalytic H_2 generation

10 mg of photocatalyst loaded with ~1 wt% Pt was added to an aqueous methanol solution (50 ml, 20%) in a closed gas circulation system. The full solar wavelength light irradiation was obtained from a 400 W Xenon lamp (Newport) embedded with IR filter. Methanol was used as a

sacrificial reagent, and the anodic reaction generating O_2 from H_2O did not occur. The amount of H_2 generated was determined by online gas chromatography (Bruker 450 GC) system connected to the reactor. The reaction was carried out at room temperature (25 °C) under Ar atmosphere. For visible light (400 to 780 nm, obtained by using a cutoff filter), 25 mg photocatalyst was used and keeping all other parameters constant. The stability of the catalyst system was studied under the full solar wavelength of light using identical reaction condition as stated above. The solution was stored in the normal ambient condition and irradiated by light for 2 h everyday up to 10 days. Then the solution was again stored for another 20 days and studied again. Before each run, the volume of the solution was made up by adding extra methanol to the solution.

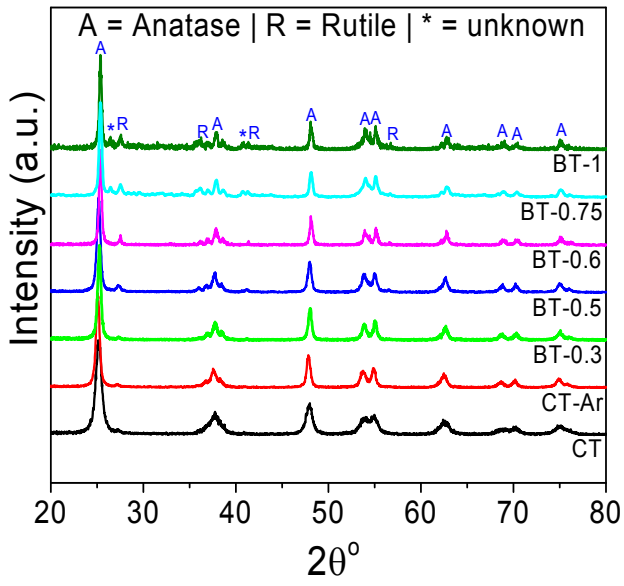

Fig. S1 Powder X-ray diffraction patterns of different samples

The XRD patterns of the different samples confirm mainly anatase phase with a little amount of rutile phase. One of the reasons for the observed rutile phase is the heating at 650 °C. Furthermore, the rutile peak is increased with the increase of Mg amount, which may indicate that the presence of Mg at high temperature also facilitates the phase transformation. The XRD pattern also indicates that the samples do not contain Mg or MgO as no related peak is observed. The XRD patterns also do not show any peak related to Ti_2O_3 or any other titanium sub-oxide. Although all the samples show a similar peak pattern, BT-0.75 and BT-1 show a few unknown peaks. These peaks are not related to Ti_2O_3, MgO or Mg_2TiO_4.

We have also calculated the crystallite size using the Scherrer equation from XRD data.

Scherrer equation	Sample	Dp (nm)
$D_p = \frac{0.94\lambda}{\beta_{1/2}\cos\theta}$ Where Dp = Average Crystallite size, β = Line broadening in radians. θ = Bragg angle λ = X-ray wavelength	CT	10.77
	CT-Ar	16.09
	BT-0.3	16.68
	BT-0.5	15.36
	BT-0.6	21. 43
	BT-0.75	25.78
	BT-1	26.36

The crystallite size of the Mg-treated samples is higher than that of pristine commercial nano TiO_2. The crystallite size of the BT-0.5 and CT-Ar is similar. This suggests that the increment of crystallite size for BT-0.5 is due to heat treatment. When higher amount (mole ratio > 0.5) of Mg is used, the crystallite size increases, which may be induced by doping of Mg.

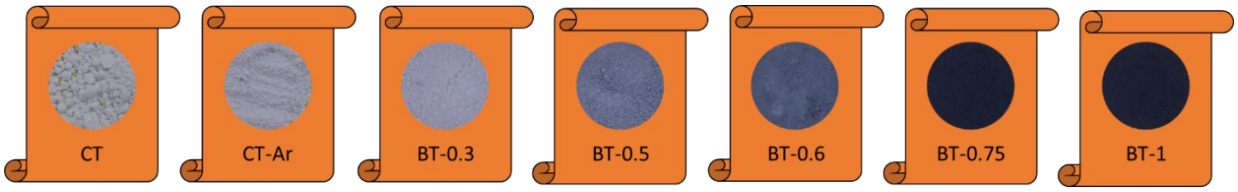

Fig. S2 Images of different samples showing corresponding color.

Although the XRD analysis does not indicate any major structural change during magnesium reduction except the introduction of rutile phase, it can be assumed that Mg changes the surface of the TiO_2 particle, which results in color change from white to gray and black with increasing Mg.

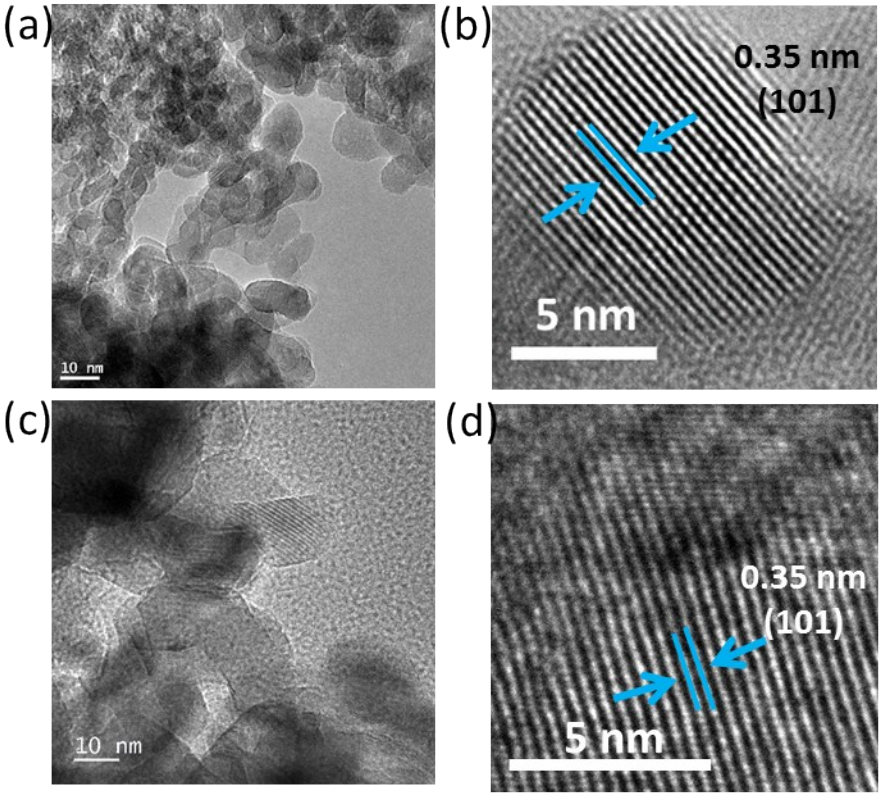

Fig. S3 HR-TEM images of CT (a and b) and BT-0.5 (c and d).

The HR-TEM images of CT and BT-0.5 show relatively small particle size. The particle size is around 10-15 nm for CT, whereas 15-20 nm for BT-0.5. This increment in particle size is considered to be due to heating at 650 °C. The lattice fringe distance is about 0.35 nm for both CT and BT-0.5, which corresponds to the (101) plane of anatase phase. It also indicates that the {101} facets are exposed for the both samples, and the exposed facet of the pristine anatase TiO_2 remains unchanged during magnesiothermic reduction. The exposed {101} facet of TiO_2 crystal is also one of the important factors for its photocatalytic performance as the surface atomic configuration and coordination effect the adsorption and reactivity.[1] In case of anatase TiO_2, {001} facets possess the highest energy and much more reactive than the thermodynamically stable {101} facets. However, in the presence of Pt as a co-catalyst, {101} facets show the highest activity for the production of hydrogen from water splitting.[2]

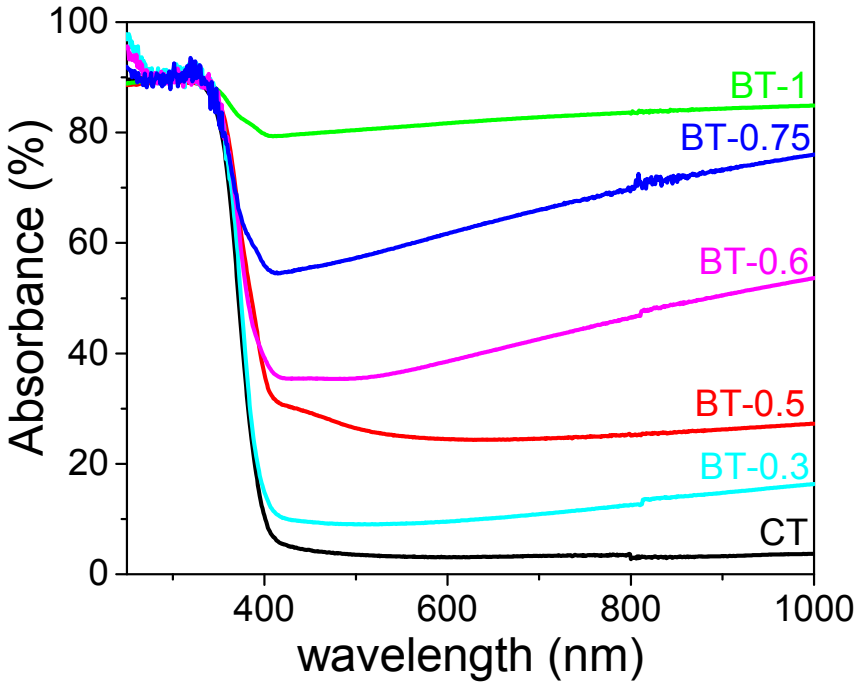

Fig. S4 Absorbance spectra of different samples.

The absorption spectra of the samples clearly depict an extended absorbance from ultraviolet (UV) to visible (VIS) and infrared (IR) region for the Mg-treated samples compared with pristine TiO_2. The absorption of light increases as the amount of Mg increases as observed for the different samples. The extended absorbance in VIS and IR region can be correlated to the color change trend of the samples from white to gray and black. Therefore, magnesiothermic treatment of titanium nanoparticles leads to surface modification, which is reflected in enhanced light absorption as well as the color change.

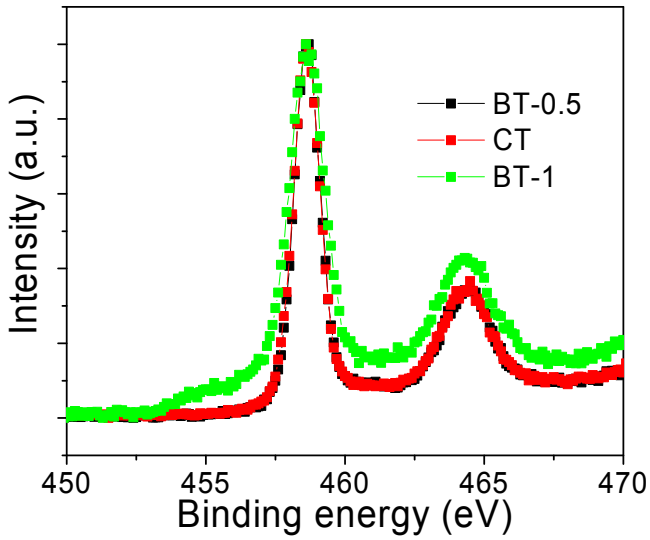

Fig. S5 Ti 2P XPS spectra of different TiO_2 samples

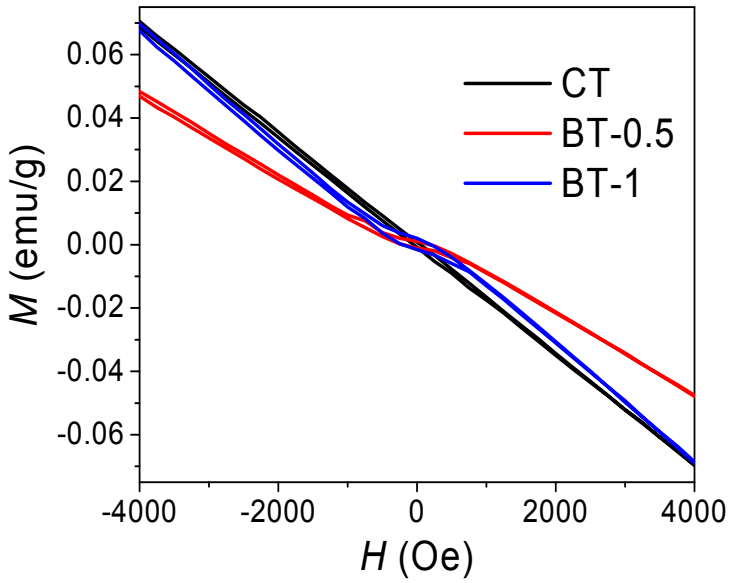

Fig. S6 Magnetic field dependence of magnetization plots of different samples.

The presence of Ti^{3+} in TiO_2 introduces ferromagnetism, which can be measured by the plot of magnetic field dependence of magnetization. The plots, corresponding to BT-0.5 and BT-1 show a clear hysteresis, while no hysteresis was observed for the pristine TiO_2 sample (CT), indicating that the ferromagnetic property is caused by the formation of Ti^{3+} in prepared samples during synthesis.

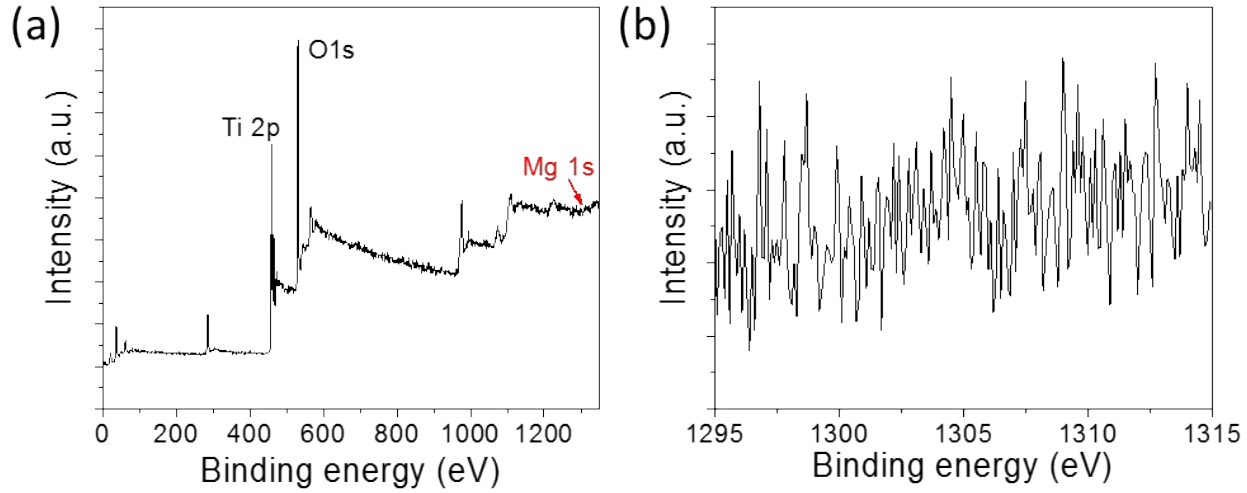

Fig. S7 Full XPS survey (a) and Mg 1s scan (b) of sample BT-0.5

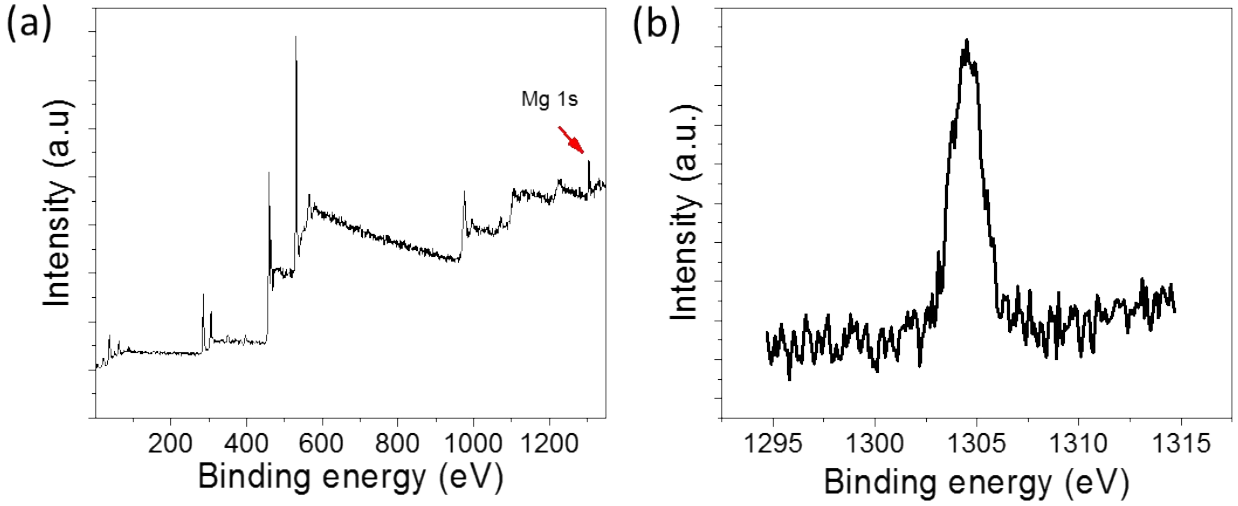

Fig. S8 Full XPS survey (a) and Mg 1s scan (b) for sample BT-1

The XPS result of sample BT-1 shows the presence of Mg in the sample. The XPS profile of Mg 1s shows a peak at 1304.5 which corresponds to Mg ion related to oxygen. As there is no peak for MgO in the XRD, the formation of Mg^{2+}-doped titanium oxide can be suggested. The formation of Mg^{2+}-doped titanium oxide is also consistent with the increment in the crystallite size of BT-1 as the ionic radius of Mg^{2+} is greater than Ti^{4+}.

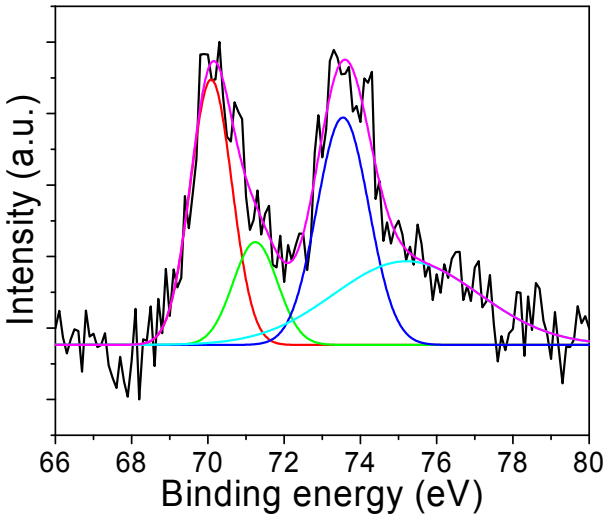

Fig. S9 XPS spectrum of Pt 4f for BT-0.5 sample after Pt deposition under UV light.

The Pt 4f XPS spectrum shows the presence of three different types of Pt species. The higher intensity components having spin–orbit split binding energies of 70.1 eV and 73.6 eV confirm the predominant presence of metallic Pt (0) states. The other two higher binding energy signals are associated with the presence of Pt(II)O and Pt(IV)O_2 species in the sample. The number ratio between loaded Pt and TiO_2 is 0.9 %.

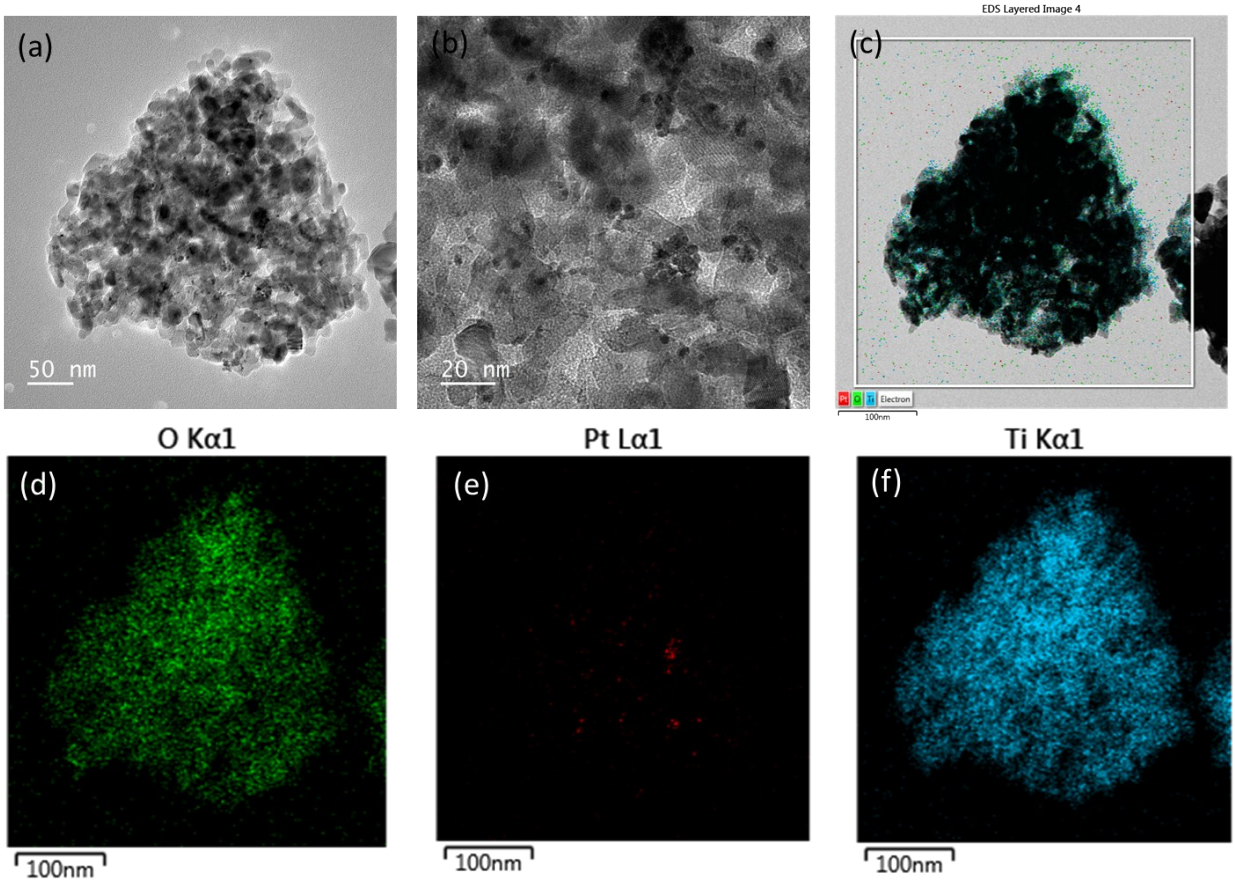

Fig. S10 HR-TEM images (a and b) and EDS elemental mappings (c-f) of Pt-deposited BT-0.5. The (c) shows the EDS layered image containing image mappings for all elements.

The HR-TEM images of Pt-deposited BT-0.5 sample show that small Pt nanoparticles (~2 nm) are homogeneously deposited on the surface of BT-0.5. The homogeneous distribution of Pt nanoparticles is further confirmed by the elemental mapping.

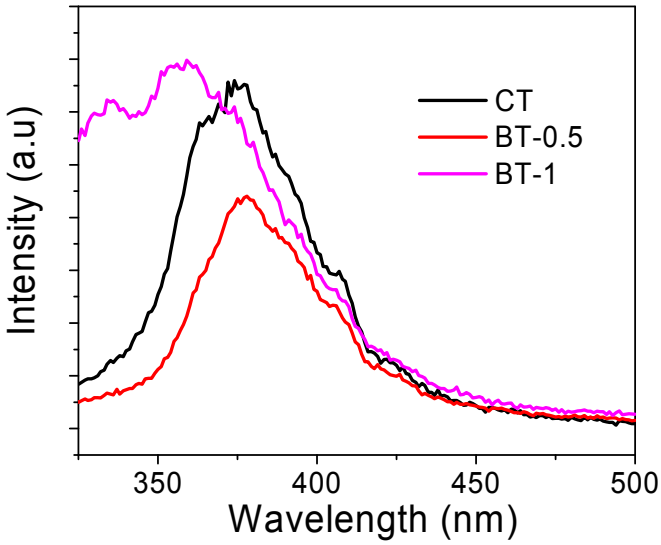

Fig. S11 Photoluminescence (PL) spectra of different samples.

To obtain the PL spectra, the sample was dispersed in ethanol (1 mg/5 ml). The excitation wavelength was 300 nm. TiO_2 is an indirect band gap semiconductor and thus does not show band gap photoluminescence. However, a broad PL spectrum was obtained due to the recombination of trapped electrons with valence band holes. The PL intensity can be directly correlated to the charge recombination. The higher intensity corresponds to the faster recombination. The PL spectra of the different samples clearly indicate much faster charge recombination for BT-1 than for BT-0.5. This result has also strong effect on the photocatalytic activity of the corresponding samples.

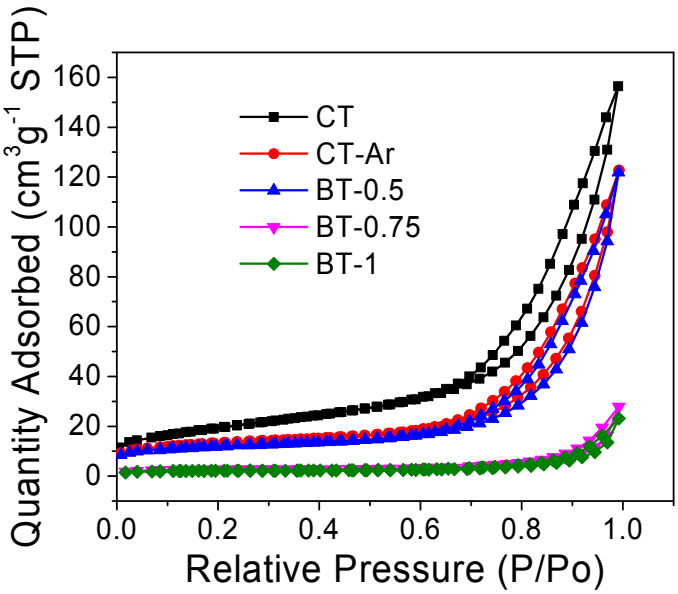

Fig. S12 N_2 adsorption/desorption isotherms for different samples.

Specific surface areas were determined by N_2 adsorption/desorption analysis. In general, it is found the surface area decreases with Mg treatment. Interestingly, the N_2 isotherms drastically change with sharp drop of surface area after the ratio of 0.5. The obtained surface areas are 69, 40, 36, 12, and 9 $m^2g^{-1}$for the sample CT, CT-Ar, BT-0.5, BT-0.75, and BT-1, respectively. The surface areas of CT-Ar and BT-0.5 are almost similar and less than that of CT. This result indicates that this decrement is mainly due to heat treatment. The drastic decrease of the surface area for the sample BT-0.75 and BT-1 can be attributed to the increase in crystallite size as observed in XRD and may be the reason behind the decrease in the rate of hydrogen production. To confirm this, we further calculate the rate of hydrogen production normalized with the surface area of the sample. The rates of hydrogen production normalized with surface area are found to be 1.2, 1.3, and 1.5 $mmolh^{-1}m^{-2}$ for BT-0.5, BT-0.75, and BT-0.1 respectively (Fig. S13).

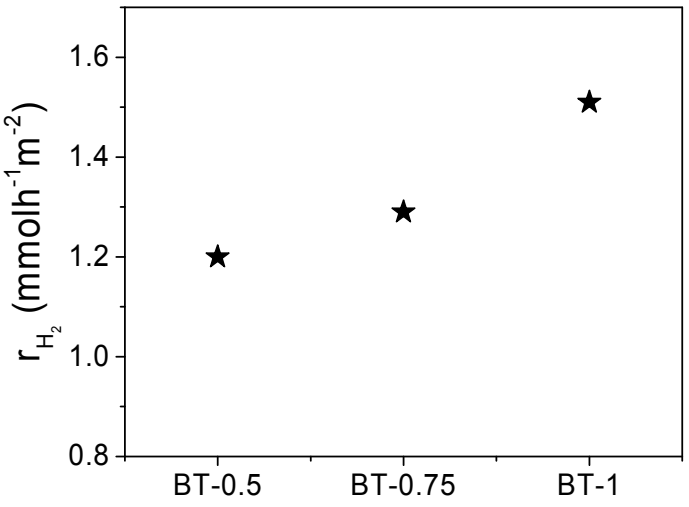

Fig. S13 Rate of surface area-normalized hydrogen generation (r_{H_2}) for different samples.

To calculate the rate of surface area-normalized hydrogen production (mmolh^{-1}m^{-2}), the rate of mass-normalized hydrogen production (mmolh^{-1}g^{-1}) is divided by the specific surface area (m^{2}g^{-1}) of the corresponding sample. The obtained results are as follow.

Sample	Rate of hydrogen production (mmolh^{-1}g^{-1})	Surface area (m^{2}g^{-1})	Rate of hydrogen production (mmolh^{-1}m^{-2})
BT-0.5	43.2	36	1.2
BT-0.75	15.4	12	1.3
BT-1	13.9	9	1.5

The results are quite interesting, showing a gradual increment of surface area-normalized rate with increase of Mg amount. Although several factors control the photocatalytic water splitting in semiconductor catalyst system, this result clearly suggests that the decrease in surface area is one of the culprits for the decrease in the rate of hydrogen production in the high Mg-treated samples like BT-0.75 or BT-1. The high surface area material can offer more active sites and improve the distribution of Pt nanoparticles to increase the overall catalytic activity. This

decrease in surface area also results in increased Pt particle size, decreasing the efficiency of Pt particles.

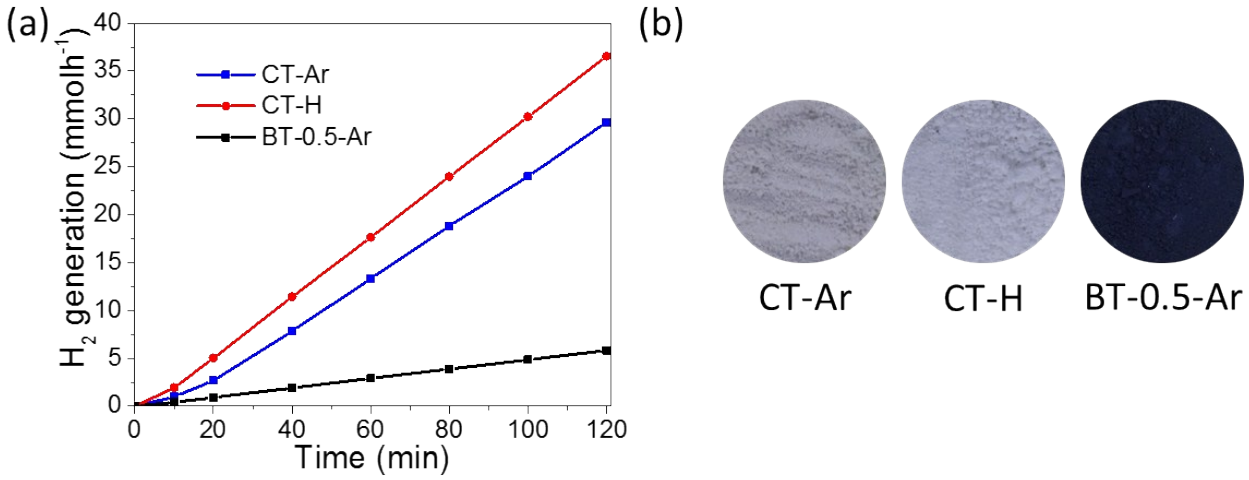

Fig. S14 (a) Hydrogen production profiles for the samples, CT-Ar, CT-H, and BT-0.5-Ar and (b) color of the corresponding samples.

To investigate the effect of Mg and H_2 on the activity of the prepared catalyst, different samples were prepared by varying the synthesis conditions (see experimental section). The rate of hydrogen productions are 15.2, 18.5, and 3 $mmolh^{-1}g^{-1}$ for the samples of CT-Ar, CT-H, and BT-0.5-Ar, respectively. The slight increase in activity of CT-H compared to CT-Ar can be due to the light hydrogenation of nano TiO_2 materials. The hydrogenation effect is very less, and the sample color is still white (same as CT) as the sample was prepared using only 5% H_2 in Ar for 5 h at 650°C. This result also suggests that the excellent photocatalytic activity of BT-0.5 is not because of this mild hydrogenation. On the other hand, interestingly, the BT-0.5-Ar shows dark black color, but reveals poor photocatalytic activity. This can be further correlated to the results obtained for BT-1. Therefore, it can be concluded that the synergy effect of Mg and hydrogen is the essential to afford the most active photocatalyst.

Table S1. Rate of hydrogen generation obtained by using different black TiO_2 materials

Black TiO_2 photocatalyst	Reactant solution	Co-catalyst	Light source	Rate of hydrogen generation	
				Full solar wavelength of light ($mmolh^{-1}g^{-1}$)	Visible light ($\mu molh^{-1}g^{-1}$)
Hydrogenated Black TiO2[3]	50 % CH_3OH	0.6 % Pt	AM-1.5 solar stimulator	10	100
Hydrogenated titanate nanotube[4]	20 % CH_3OH	1 % Pt	Xe arc lamp, 300 W	2.15	120
Al-reduced black TiO_2[5]	25 % CH_3OH	0.5 % Pt	Hg lamp, 300W	6.4	140
Nonmetal doping Al-reduced black TiO_2[6]	20 % CH_3OH	0.5 % Pt	Xe lamp, 300 W		
TiO2-H				7.4	123
TiO2-N				15	200
TiO2-S				12.1	135
TiO2-I				10.3	160
Al-reduced black S doped rutile TiO_2[7]	50 % CH_3OH	0.5 % Pt	AM 1.5 simulated solar power system	---	258
Ordered mesoporous hydrogenated black TiO_2[8]	20 % CH_3OH	1 % Pt	AM 1.5 solar power system	---	13.6
Current work	20 % CH_3OH	1 % Pt	Xe lamp, 400 W	43.2	440

References

1 J. Yan, G. Wu, N. Guan, L. Li, Z. Li and X. Cao, *Phys. Chem. Chem. Phys.*, 2013, **15**, 10978-10988.

2 T. R. Gordon, M. Cargnello, T. Paik, F. Mangolini, R. T. Weber, P. Fornasiero and C. B. Murray, *J. Am. Chem. Soc.*, 2012, **134**, 6751-6761.

3 X. Chen, L. Liu, P. Y. Yu and S. S. Mao, *Science*, 2011, **331**, 746-750.

4 Z. Zheng, B. Huang, J. Lu, Z. Wang, X. Qin, X. Zhang, Y. Dai and M.-H. Whangbo, *Chem. Commun.*, 2012, **48**, 5733-5735.

5 Z. Wang, C. Yang, T. Lin, H. Yin, P. Chen, D. Wan, F. Xu, F. Huang, J. Lin, X. Xie and M. Jiang, *Energy Environ. Sci.*, 2013, **6**, 3007-3014.

6 T. Lin, C. Yang, Z. Wang, H. Yin, X. Lu, F. Huang, J. Lin, X. Xie and M. Jiang, *Energy Environ. Sci.*, 2014, **7**, 967-972.

7 C. Yang, Z. Wang, T. Lin, H. Yin, X. Lü, D. Wan, T. Xu, C. Zheng, J. Lin, F. Huang, X. Xie and M. Jiang, *J. Am. Chem. Soc.*, 2013, **135**, 17831-17838.

8 W. Zhou, W. Li, J.-Q. Wang, Y. Qu, Y. Yang, Y. Xie, K. Zhang, L. Wang, H. Fu and D. Zhao, *J. Am. Chem. Soc.*, 2014, **136**, 9280-9283.